UDK 679.743.1:620.181
Original scientific article/Izvirni znanstveni članek

ISSN 1580-2949
Mater. Tehnol.

PERFORMANCE OPTIMIZATION AND MOLECULAR DYNAMICS MECHANISM OF COMPOSITE INSULATING SILICONE RUBBER AFTER ELECTRIC HEATING POST-TREATMENT

OPTIMIZACIJA LASTNOSTI IN MEHANIZEM MOLEKULARNE DINAMIKE KOMPOZITNE SILIKONSKE GUME PO NAKNADNI OBDELAVI Z ELEKTRIČNIM OGREVANJEM

Pengkang Xie*, Kai Ning, Zhenglong Jiang

State Key Laboratory of Power Grid Disaster Prevention and Reduction (Disaster Prevention and Reduction Center of State Grid Hunan Corporation), Changsha 410000, Hunan, China

Prejem rokopisa – received: 2025-09-20; sprejem za objavo – accepted for publication: 2026-01-22

doi:10.17222/mit.2025.1568

This study investigates the optimization of composite silicone rubber (SR) through a physical electrothermal post-treatment process that functions as an efficient structural annealing method. The aim is to enhance the material's intrinsic properties without relying on formulation modifications. Experimental results show that post-treatment at 300 °C for 1 h significantly improved the material's mechanical properties, achieving a simultaneous increase in stiffness and toughness: tensile strength and Young's modulus (YM) rose by ≈45 % (to 14.9 MPa) and ≈56 % (to 0.75 GPa), respectively, while elongation at break improved to 391 %. Molecular dynamics (MD) simulations were employed to understand the microscopic mechanisms behind these improvements. The post-treatment process increased the crosslink density (CD) from 78 % to 92 %, leading to a densified molecular chain network, with a reduction in the free volume fraction (FVF). The simulated YM growth (+49 %) closely matched the experimental increase (+56 %), confirming that crosslink network optimization was the main contributor to performance enhancement. Thermal performance analysis revealed that the glass transition temperature (Tg) increased from –48.5 °C to –42.1 °C, alongside an improvement in thermal stability. Electrical properties also improved, with a reduction in the dielectric constant and an increase in insulation resistance by ≈24 % (to 310.7 MΩ). This study demonstrates that electrothermal post-treatment, guided by MD simulations, effectively enhances the performance of SR, offering a reliable endogenous optimization alternative to traditional additive-based modification techniques.

Keywords: electrical post-treatment, composite insulating silicone rubber, molecular dynamics, performance optimization

V članku avtorji opisujejo študijo, ki raziskuje optimizacijo kompozitne silikonske gume (SR) s fizikalno elektrotermičnim postopkom naknadne obdelave, ki deluje kot učinkovita metoda strukturnega žarjenja. Cilj avtorjev je bil izboljšati notranje (intrinzične, strukturne) lastnosti materiala brez zanašanja na modifikacije njene formulacije (sestave). Eksperimentalni rezultati so pokazali, da enourna naknadna obdelava pri 300 °C znatno izboljša mehanske lastnosti materiala, pri čemer se je doseglo hkratno povečanje togosti in žilavosti: natezna trdnost in Youngov modul (YM) sta se povečala za približno 45 % (na 14,9 MPa) oziroma približno 56 % (na 0,75 GPa), medtem ko se je raztezek pri pretrgu izboljšal za 391 %. Za razumevanje mikrostrukturnih mehanizmov, ki so vzrok za te izboljšave, so bile uporabljene simulacije molekularne dinamike (MD). Postopek naknadne obdelave je povečal gostoto zamreženja (CD) z 78 % na 92 %, kar je vodilo do zgoščene mreže molekularnih verig z zmanjšanjem deleža prostega volumna (FVF). Simulirana rast YM (+49 %) se je tesno ujemala z eksperimentalnim povečanjem (+56 %), kar potrjuje, da je optimizacija zamreženja glavni dejavnik pri izboljšanju zmogljivosti. Analiza toplotne zmogljivosti je pokazala, da se je temperatura steklastega prehoda (Tg) povečala z –48,5 °C na –42,1 °C, hkrati pa se je izboljšala tudi toplotna stabilnost. Izboljšale so se tudi električne lastnosti, z zmanjšanjem dielektrične konstante in povečanjem izolacijske upornosti za približno 24% (na 310,7 MΩ). S to študijo so avtorji dokazali, da elektrotermična naknadna obdelava, ki jo vodijo MD simulacije, učinkovito izboljša delovanje SR in ponuja zanesljivo alternativo "endogene optimizacije!" tradicionalnim tehnikam modifikacije na osnovi dodatkov.

Ključne besede: naknadna obdelava z električnim ogrevanjem, kompozitna izolacijska silikonska guma, molekularna dinamika, optimizacija zmogljivosti

1 OVERVIEW

High-performance insulating materials are becoming more and more in demand in industries like electronics, energy, and aerospace due to the quick advancement of contemporary industrial technologies. Composite insulating silicone rubber (SR) materials are widely used in various high-demand scenarios due to their excellent insulating properties, thermal stability, and mechanical properties (MPs).[1,2] However, traditional SR materials still have certain limitations in terms of performance under high temperatures, high voltages, and complex environments.

In recent years, researchers have conducted modification studies on SR materials using a variety of methods. These strategies can be broadly categorized into two main directions: the first focuses on formulation-centric approaches, such as adding nanofillers, using plasticizers, introducing new fillers, or improving filler disper-

*Corresponding author's e-mail:
XiePengkang@sklpgdpr.org.cn (Pengkang Xie)

sion to enhance performance.[3,4] The second is production process optimization, such as using machine learning to enable intelligent control of the production process.[5,6]

Y. Yang addressed the issues of complex, inefficient, and unstable quality in traditional SR production processes by proposing a production process optimization method based on machine learning. The outcomes revealed that this method could significantly improve production efficiency, reduce defect rates, and decrease raw material waste and energy consumption.[7] Leong et al. addressed the current situation where the application of graphene in rubber formulations affects the performance of nanocomposites. They proposed a method to improve the dispersion of graphene through intense mixing techniques such as mechanical stirring, grinding, and ultrasonication, while also utilizing response surface methodology to optimize graphene nanocomposites. The outcomes revealed that these methods effectively improved the dispersion of graphene in rubber and enhanced the mechanical, electrical, and thermal properties of the composites.[8] Xie et al. addressed the issues of insufficient MPs and thermal stability in traditional silica/SR composite materials by proposing a method for preparing montmorillonite nanotube-silica nanocomposite fillers using an in situ assembly process. The results showed that the composite material exhibited optimal dispersion and the weakest filler network structure at a fixed filler loading, with a tensile strength of 6.2 MPa. Additionally, the fracture elongation of the nanocomposite reached 418 %, which was 1.67 times that of silica/SR composites with the same filler loading, and both tear strength and hardness were also improved.[9]

Although the above studies have made positive progress, the existing research paradigm has its inherent limitations. The formulation optimization strategy often faces challenges such as poor compatibility between new fillers and the matrix interface, increased process complexity, and higher costs. Meanwhile, production process optimization mainly focuses on the efficiency and uniformity of the molding process, with limited potential for exploiting the inherent properties of cured molded materials. Therefore, a key scientific question arises: without altering the existing chemical composition of the material, is it possible to use a controlled physical post-processing method to perform secondary structural annealing on the formed composite material in order to unlock its untapped performance potential?

Unlike traditional convective-oven post-curing, which often suffers from slow heat transfer and energy inefficiency, the electrothermal post-treatment method proposed herein utilizes a resistive heating element embedded within or in direct contact with the material. This approach allows for rapid, in-situ treatment of components and ensures efficient, direct thermal energy transfer to the polymer network. Although post-curing processes are used in industry, they are often regarded as ancillary steps in the production process. The synchronous effects of post-curing on the multi-physical properties (mechanical, thermal, and electrical) of composite SR systems, as well as the microscopic physical mechanisms involved in the transition from a metastable network to a stable network, remain a systematic gap in academic research, particularly at the molecular dynamics (MD) level.

Based on this, the study proposes an optimization strategy for composite-insulating SR materials. This strategy combines electrothermal post-treatment with MD simulation technology. The goal is to reveal the intrinsic microscopic mechanism of performance improvement. This study's primary innovation is that it is the first to approach post-processing as a separate, controllable physical-modification tool and to isolate it from the production process. The study systematically elucidates how the microstructural evolution from a metastable crosslinked network to a stable network directly translates into an improvement in macroscopic mechanical, thermal, and electrical properties. This improvement is achieved through computational simulations and provides a solid theoretical and experimental basis for transcending traditional additive modification approaches.

2 METHODS AND MATERIALS

2.1 Laboratory reagents and instruments

Table 1 lists the primary resources used in this investigation.

Table 2 lists the devices and equipment utilized in the experiment along with the experimental ingredients.

Table 1: Experimental materials and reagents

Material/reagent	Type/description	Purity/specification	Manufacturer
SR matrix	Vinyl-terminated polydimethylsiloxane (PDMS)	Molecular weight: 150,000 g/mol	Dow Inc. (USA)
Nano-silica	Fumed silica, hydrophobic	Particle size: ≈10 nm, Specific surface area: ≈200 m^2/g	Evonik Industries (Germany)
Vinyl silicone oil	Vinyl-terminated PDMS oil	Molecular weight: 8000 g/mol	Wacker Chemie AG (Germany)
Curing agent	Platinum catalyst system	-	Dow Inc. (USA)
Electric heating element	Nickel-chromium alloy wire	Diameter: 0.5 mm	Alfa Aesar (USA)
Ethanol	Solvent for ultrasonic dispersion	Analytical grade, ≥99.7 %	Sinopharm Chemical Reagent Co., Ltd. (China)

Table 2: Experimental equipment

Equipment/instrument	Model/specification	Manufacturer
Ultrasonic disperser	JY92-IIN, Power: 200 W	Ningbo Scientz Biotechnology Co., Ltd. (China)
Two-roll mill	XK-160	Dongguan Lixian Instrument Technology Co., LTD (China)
Molding press	XLB-D 50T	
Differential scanning calorimeter	TA Instruments Q20	TA Instruments (USA)
Thermogravimetric analyzer	TA Instruments Q50	
Tensile testing machine	Instron 5967, Gauge length: 50 mm	Instron (USA)
Compression testing machine	Instron 5967, Sample: Ø10 × 20 mm	Instron (USA)
Shore hardness tester	LX-D Shore Durometer	Shanghai Yizong Precision Instrument Co., LTD (China)
Dielectric constant tester	Keysight E4980A LCR Meter	Keysight Technologies (USA)
Insulation resistance tester	Keysight B2985A Electrometer	Keysight Technologies (USA)
Scanning electron microscope (SEM)	Zeiss Gemini SEM 500	Carl Zeiss AG (Germany)

2.2 Composite material preparation method

The composite material system is based on a SR matrix (100 parts), nanosilica (10 parts), and vinyl silicone oil (5 parts). The preparation process is displayed in **Figure 1**.

Pre-treatment and mixing: Prior to use, the SR matrix was dried for 4 h at 80 °C in a vacuum oven. The nanosilica filler was dispersed in ethanol using a 200 W ultrasonic disperser for 30 min to ensure uniform dispersion.[10,11] Next, the dried SR matrix was processed in a twin-roll open mill (roll gap: 1 mm, speed ratio: 1:1.2) at 150 °C. The ultrasonically dispersed nanosilica and vinyl silicone oil were added sequentially and mixed for 60 min until a uniform compound was obtained.

Compression molding: The uniformly mixed compound was placed in a mold at 180 °C and held at a pressure of 10 MPa for 10 min to cure, forming a (100 × 100 × 2) mm sample.

Electrothermal post-treatment: The molded composite material sample was placed in a specially designed electric heating treatment device. By applying a precisely controlled current to the embedded nickel-chromium alloy heating element (temperature control accuracy: ±1 °C), the sample was heated to 300 °C in an airtight environment. To ensure thermal homogeneity, the heating element layout was optimized to a serpentine pattern, covering the entire sample area to minimize temperature gradients. The sample was maintained at this constant temperature for 1 h.

The process parameters were determined based on a series of preliminary experiments. The effect of treatment temperature (250–325 °C) and time (0.5–2 h) on tensile strength was examined. Results revealed that performance improvement was not significant below 280 °C, while temperatures above 320 °C caused slight yellowing, indicating the onset of thermal degradation. Consequently, 300 °C was selected as the optimal temperature – sufficiently high to activate residual cross-linking sites (being below the initial decomposition temperature of ≈350 °C determined by TGA) yet safe enough to maintain stability. Regarding time, performance improvements plateaued after 1 h; thus, 1 h was chosen to balance efficiency and effectiveness. After processing, the sample was cooled to room temperature (RT) within the device, then cut and polished to prepare standard test specimens.

2.3 Material systems and microstructures

This study constructs a composite material system composed of a SR matrix, nanosilica filler, and vinyl sili-

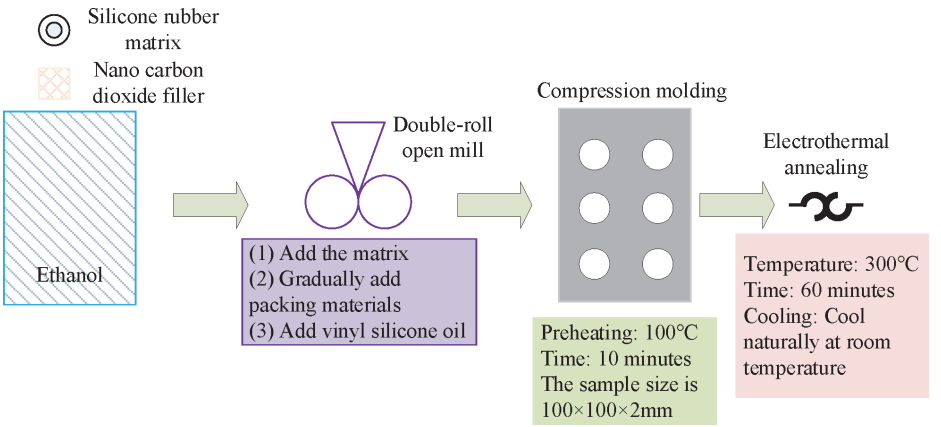

Figure 1: Preparation process of the composite material

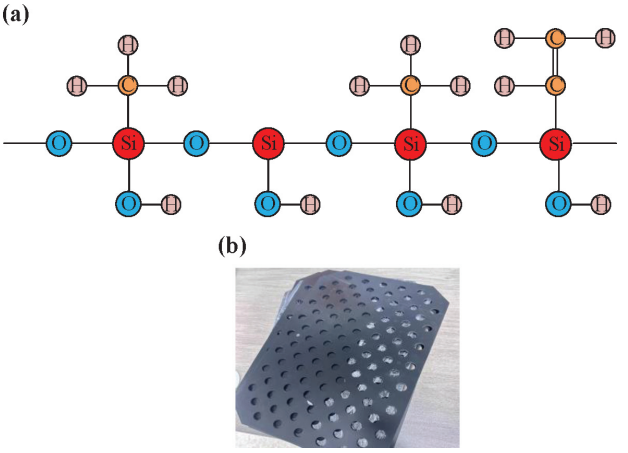

Figure 2: Schematic diagram of the: a) silicone rubber molecular chain and b) composite insulating SR material

cone oil plasticizer. The prepared high-performance composite insulating SR material is used as the research object, and its performance is optimized through electrothermal post-treatment. The composite insulating SR material and molecular chain structure are shown in **Figure 2**.

In **Figure 2**, the main chain of the SR matrix is primarily composed of siloxane bonds, while the side chains are connected to methyl and vinyl groups. This structure confers excellent flexibility and heat resistance to SR.[12,13] Through electrothermal post-treatment, the molecular chains are expected to exhibit a higher crosslink density and a more ordered structure. The molecular structural changes of the SR molecular chains during electrothermal post-treatment are shown in **Figure 3**.

To further enhance the performance of composite materials, various additives are used in this research. Among these, nanosilica serves as an important filler, with a particle size of approximately 10 nm, featuring a high specific surface area and excellent dispersibility. Additionally, a small amount of vinyl silicone oil is added as a plasticizer to improve the processability and flexibility of SR. The addition of vinyl silicone oil is controlled at around 5 % of the SR's mass. This ratio effectively improves processing performance without significantly reducing the material's insulation properties. The addition of the plasticizer helps improve molecular chain mobility during processing and facilitates the formation of a more uniform cross-linked network during the subsequent heat treatment.

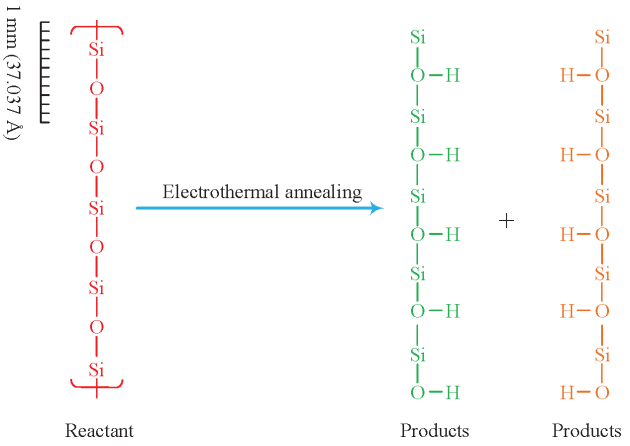

Figure 3: Schematic diagram of molecular network evolution and annealing mechanism during electrothermal post-treatment

2.4 MD simulation method

In terms of simulation software and platforms, the study uses a large-scale atomic/molecular massively parallel simulator (LAMMPS) as the main tool for MD simulation.

Model construction: To conceptually validate that crosslink density (CD) is the core mechanism determining performance changes, this study employs a steady-state comparison strategy rather than precisely reproducing complex dynamic chemical reaction processes. This strategy aims to accurately isolate the influence of CD as a single variable on macro performance. Therefore, this study constructs two idealized models representing the pre-treatment and post-treatment states, respectively. The key difference lies in their CD. To determine specific CD values, we referred to fundamental polymer physics principles. First, regarding the pre-treatment state, it is well-established that steric hindrance and topological constraints (such as chain entanglement) often prevent a complete reaction of functional groups during standard curing, resulting in a metastable network with a conversion typically limited to 70–80 %.[14] Second, for the post-treatment state, recent studies on the thermal history of PDMS have experimentally demonstrated that elevated curing temperatures significantly enhance the final crosslink density by providing the activation energy required to overcome mobility restrictions.[15] While the theoretical upper limit of CD is 100 %, in practice, topological locking prevents the formation of a perfect network. Therefore, based on these mechanisms, this study sets a crosslink density of 78 % as the representative pre-treatment/metastable state model and a crosslink density of 92 % as the post-treatment/stable state model (representing a near-saturation level). This 14 % differential was chosen as being sufficiently distinct to perform a sensitivity analysis on how network densification impacts performance. Although the actual cross-linking process is dynamic and complex, the core objective of this study is to reveal the decisive influence of the core variable of the crosslink density on the final performance. By comparing the performance differences between these two static models, this study can effectively link the optimization of the cross-linking network structure with the improvement of macro performance. Crucially, this theoretical assumption of network densification is strongly corroborated by our subsequent experimental results (Section 3.2). According to the classical theory of rubber elasticity ($E \propto v_e$), the substantial increase in the experimental

Young's modulus (+56 %) serves as a direct macroscopic proxy for the increase in the crosslink density, validating the trend captured by the chosen simulation parameters (78–92 %). CD is defined here as the percentage of potential crosslinking sites that have formed covalent bonds out of the total number of potential crosslinking sites in the system.

Force field and potential function: The optimized potentials for liquid simulations (OPLS-AA) force field are used to describe interatomic interactions within the system. This force field accurately handles molecular conformations and non-bonded interactions, making it suitable for analyzing the performance of systems with defined chemical bonding relationships.

Simulated process:

1. Initial structure generation: Based on the above two crosslink densities, amorphous simulation boxes containing all components are constructed.

2. Minimizing energy: The conjugate gradient method is used to minimize the energy of the initial structure in order to eliminate unreasonable contacts and high-energy configurations until the energy gradient is less than 1.0×10^{-3} eV nm^{-1}.

3. System balance: First, under NVT ensemble conditions (constant particle number, volume, and temperature), a relaxation of 10 ns is performed at 300 K to ensure uniform system temperature. Subsequently, the system is switched to NPT ensemble conditions (constant particle number, pressure, and temperature), and relaxation is continued for 10 ns at 1 atm and 300 K to achieve true density and pressure equilibrium.

4. Production simulation and performance calculation: A production simulation of 80 ns is performed on the balanced system. At this stage, the stress-strain response is recorded by applying uniaxial tensile deformation to the simulation box, thereby calculating the Young's modulus (YM). The structural parameters of the system (such as free volume fraction (FVF) and radial distribution function) are also continuously tracked and analyzed. Specifically, the FVF was calculated using the Connolly surface method with a probe radius of 0.1 nm to define the void space accessible to penetrants.

By comparing the simulation results of these two preset models with different crosslinking degrees, it is possible to effectively reveal how the optimization of the microscopic network structure directly leads to improvements in the macroscopic performance.

2.5 Performance testing methods

To ensure the comprehensiveness of the experiment, the performance testing methods used in the study include microstructural characterization, mechanical property testing (PT), thermal PT, and electrical PT. All performance tests are performed on two sets of samples: one before treatment and one after treatment. To ensure statistical reliability, each test is conducted on ten parallel samples (n = 10), and the results are expressed as the mean ± standard deviation (mean ± SD).

2.5.1 Microscopic morphology characterization

The sectional microstructure of the material is observed using a SEM. Before observation, the sample is first brittle fractured in liquid nitrogen to expose its internal structure, and then the section is treated with gold spraying to enhance conductivity.

2.5.2 MPs testing

Mechanical PT includes tensile PT, compression PT, and hardness testing. In tensile PT, the gauge length is 50 mm, and the tensile speed is set to 500 mm min^{-1}. In compression PT, the sample size is a cylindrical shape with a diameter of 10 mm and a height of 20 mm. The test standard is ASTM D575, and the compression speed is set to 2 mm min^{-1}. In the hardness test, a Shore hardness tester is used, and the test standard is ISO 868. Five distinct locations are used to assess each sample's hardness, and the average value is used as the final outcome. Mechanical PT provides insight into the strength, toughness, and wear resistance of materials. Optimizing MPs is critical to the reliability and service life of materials under mechanical loads.

2.5.3 Thermal performance testing

The standard for differential scanning calorimetry (DSC) testing in thermal performance testing is ASTM E1356. The sample mass is approximately 10 mg, the test temperature range is –50 to 300 °C, and the heating rate is 10 °C min^{-1}. The standard for TGA testing is ASTM E2550. The sample mass is approximately 10 mg, the test temperature range is RT to 800 °C, and the heating rate is 10 °C min^{-1}. The glass transition temperature (Tg) is determined as the midpoint of the step transition in the heat flow curve.

2.5.4 Electrical performance testing

Electrical performance testing mainly includes dielectric constant testing and insulation resistance testing. The standard for dielectric constant testing is ASTM D150, with a sample thickness of 2 mm and a test frequency range of 100 Hz to 1 MHz. The standard for insulation resistance testing is IEC 60243, with a sample thickness of 2 mm and a test voltage of 1000 V. The test results for dielectric constant and insulation resistance reflect the insulation capacity and electrical conductivity of materials in an electric field. Optimizing electrical properties facilitates the application of materials in high-voltage environments.

3 RESULTS

3.1 MD simulation results

To reveal the mechanism by which electrothermal post-treatment enhances material performance at the microscopic level, this study conducts MD simulations on

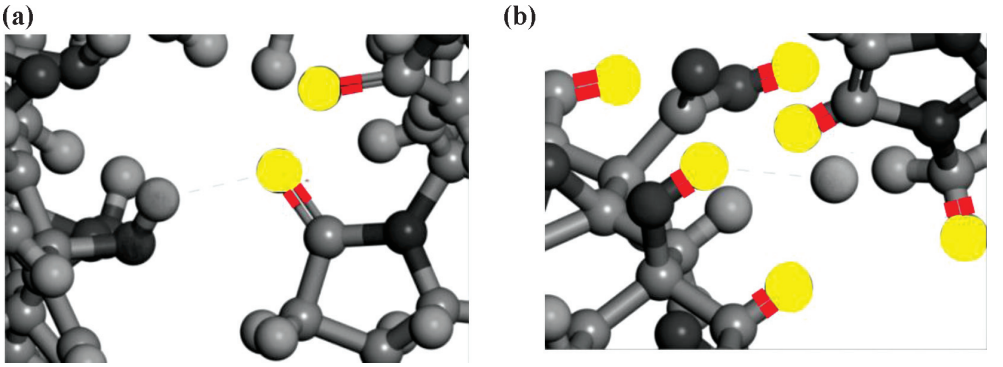

Figure 4: MD simulation comparison of composite materials' microstructures: a) before electrothermal post-treatment and b) after electrothermal post-treatment

models representing the two states, before and after treatment. The simulation results clearly show the differences in the microstructure under different crosslink networks, as shown in **Figure 4**.

Figure 4a shows the pre-treatment model with a CD of 78 %, displaying a random mixture of SR molecular chains (gray) and nanosilica fillers (yellow spheres), with a relatively loose network structure. **Figure 4b** shows the treated model with a CD of 92 %. It can be observed that a denser crosslink network (red bonds) has formed between the molecular chains, resulting in a more compact and regular overall structure.

Quantitative analysis further confirms the impact of structural optimization on the performance. Through simulated tensile testing of the two models, the calculated YM increases from 0.55 GPa in the pre-treatment model to 0.82 GPa in the post-treatment model. Although the absolute value of the YM calculated from the simulation is slightly higher than the experimental value due to model idealization (which lacks microdefects and inhomogeneity inevitably present in macroscopic samples), the growth trend (49 % increase obtained with the simulation) is highly consistent with the subsequent macroscopic experimental results (56 % increase obtained with the experiment). In addition, the study calculates the FVF of the model. The results show that processing significantly reduces the FVF from 5.8 % in the pre-processing model to 4.1 % in the post-processing model. The densification of molecular packing provides direct microscopic evidence for the subsequent improvement in the electrical and thermal performance. In summary, MD simulations provide strong microscopic evidence for the core hypothesis that žincreased crosslink density and structural densification are the fundamental causes of performance enhancement.'

3.2 Mechanical performance analysis

The effectiveness of electrothermal post-treatment in improving the mechanical properties of the materials can first be verified by changes in the microstructure. In **Figure 5**, the frozen fracture surface (a) of the sample before treatment is relatively rough, which may reflect the unevenness of the internal network stress transfer. In contrast, the cross-section of the treated sample (b) is significantly smoother and denser. Although the fracture morphology itself is influenced by a variety of factors, this visual improvement indirectly indicates that a more uniform and stable cross-linked network has been

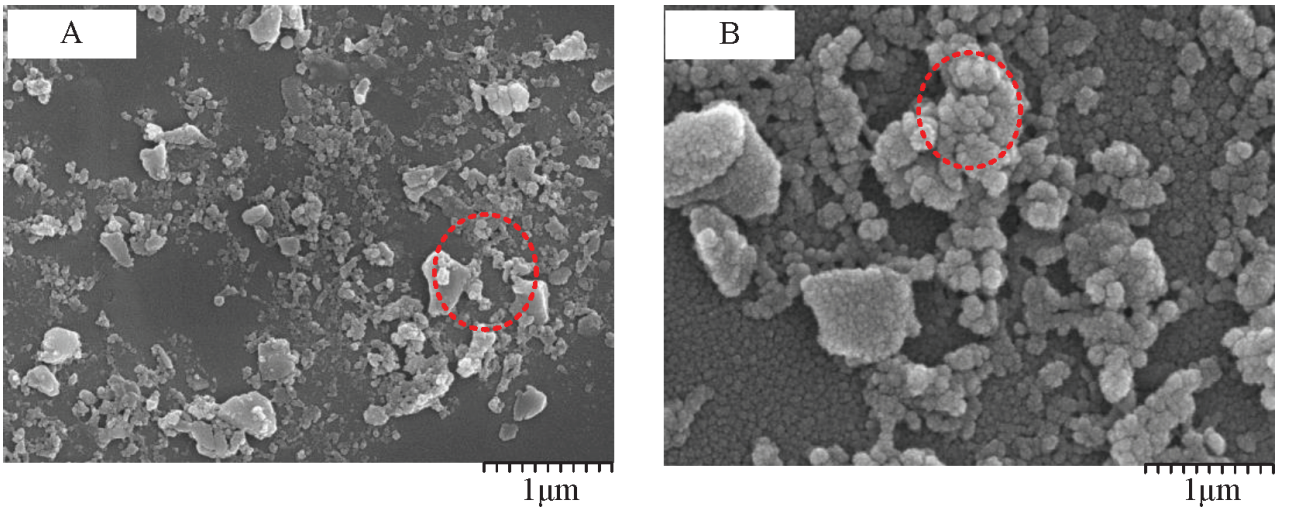

Figure 5: SEM images of composite materials: a) before electrothermal post-treatment and b) after electrothermal post-treatment

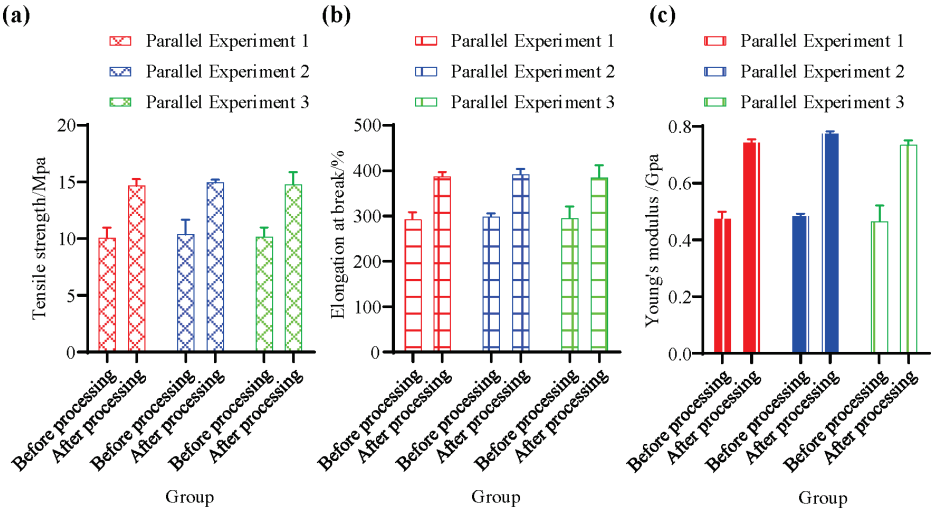

Figure 6: Comparison of: a) tensile strength values, b) elongation at break values and c) YM indicators

formed, which is highly consistent with the significant enhancement of macro-mechanical properties.

This optimization of the microstructure directly leads to a significant enhancement in macroscopic mechanical properties (the error bars in **Figures 6–8** represent standard deviations). The tensile strength rises by 44.7 %, from 10.3 MPa to 14.9 MPa (**Figure 6a**). It is worth noting that this magnitude of improvement is superior to several recent studies focusing on formulation optimization, where improvements often range from 10–25 %.[3–9]

The elongation at break increases from 298 % to 391 %, an increase of 31.2 % (**Figure 6b**), indicating enhanced material toughness. The YM increases from 0.48 GPa to 0.75 GPa (**Figure 6c**), indicating a significant increase in stiffness. Typically, in polymer composites, an increase in stiffness (YM) is accompanied by a decrease in ductility (elongation at break). However, the simultaneous improvement of both properties in this study suggests a highly successful synergistic reorganization of the network. The post-treatment effectively eliminates local stress concentrations and defects, allowing the network to bear higher loads while maintaining the flexibility to deform.

Figure 7 compares the compression performance before and after treatment. In **Figure 7a**, the average compression strength before treatment is 20.0 MPa, which increases to 24.9 MPa after treatment, representing an average increase of 24.5 %. This indicates that the material's load-bearing capacity under pressure has been significantly enhanced. In **Figure 7b**, the compressive modulus then increases significantly from 0.29 GPa before treatment to 0.49 GPa, an average increase of 63.3 %. This shows that the stiffness of the material under pressure is significantly enhanced.

Figure 8 compares the Shore hardness before and after treatment. The average Shore hardness before treatment is 31.6 Shore D, and the average Shore hardness after treatment is 39.3 Shore D. The hardness is increased significantly, with an average increase of 23.4 %. This indicates that the surface hardness of the material is significantly enhanced, and its wear resistance and scratch resistance are improved.

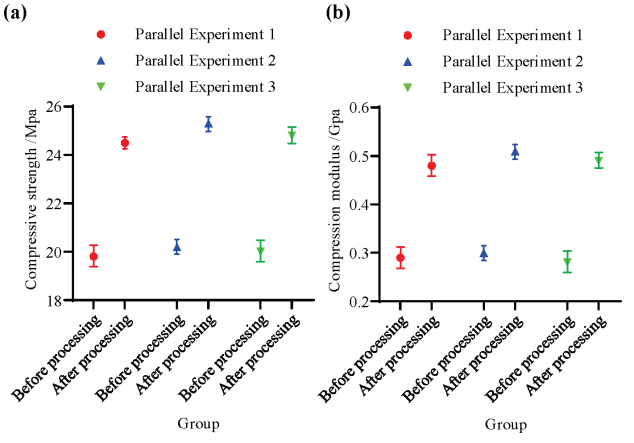

Figure 7: Compression performance comparison including: a) compressive strength and b) compression modules

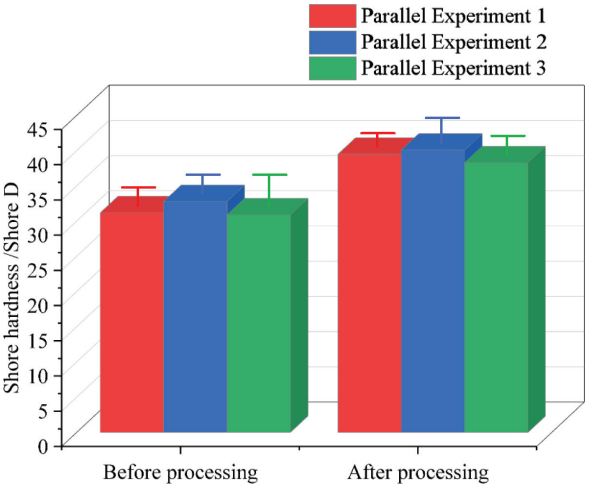

Figure 8: Comparison of Shore hardness before and after treatment

This comprehensive enhancement in macroscopic mechanical behavior is fully consistent with the microscopic mechanism predicted by MD simulations, namely improved stress transfer efficiency and network uniformity due to increased CD (78 → 92 %).

3.3 Analysis of thermal performance test results

Consistent with the enhancement of mechanical properties, the thermal stability of the material is also significantly improved through post-treatment. The DSC curves before and after treatment are shown in **Figure 9**. The glass Tg of the material before treatment is –48.5 °C. After electrothermal post-treatment, the Tg is significantly increased, to –42.1 °C. An increase in Tg directly reflects the macroscopic effect of restricted molecular chain movement. This strongly indicates that the dense network structure formed by post-treatment limits the cooperative movement capability of the chain segments.

The TGA results of the material (**Figure 10**) further confirm the enhanced thermal stability. The curves of the treated samples are overall shifted toward the high-temperature region, indicating that their thermal stability is significantly better than that of the untreated samples. Specifically, the initial decomposition temperature of the untreated samples is approximately 340 °C, while that of the treated samples is increased to approximately 375 °C. The treated samples' mass loss rate is continually lower than that of the untreated samples during heating. At 800 °C, the final residual carbon content of the untreated sample is 89.22 %, while that of the treated sample is 90.49 %. The higher residual carbon content also demonstrates its superior thermal stability. This enhanced char yield is attributed to the higher crosslink density, which promotes the formation of a compact carbonaceous layer during decomposition. This layer acts as a physical barrier, retarding the volatilization of degradation products and protecting the underlying matrix.

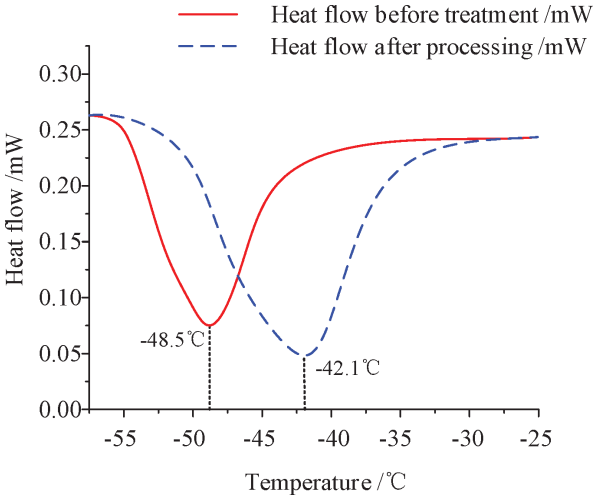

Figure 9: Comparison of differential calorimetric scanning curves before and after treatment

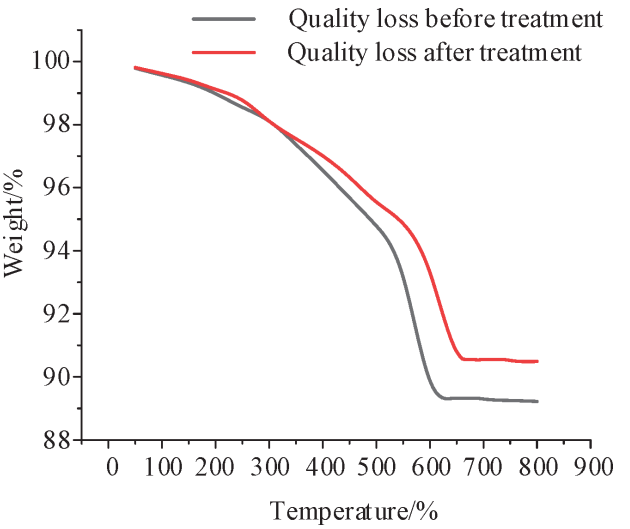

Figure 10: Comparison of TGA results

These results indicate that electrothermal post-treatment effectively inhibits molecular chain breakage and degradation at high temperatures by constructing a more stable cross-linked network.

The increase in Tg and the rise in thermal decomposition temperature once again confirm the conclusions of the MD simulation from an energy perspective – a denser cross-linked network enhances the confinement of molecular chain segment motion, thereby improving the overall thermal stability of the system.

3.4 Electrical performance test results

In addition to its excellent mechanical and thermal properties, electrothermal post-treatment also significantly enhances the core electrical properties of the material as an insulator. As shown in **Table 3**, the dielectric constant is 3.12 at 100 Hz and 2.76 at 1,000,000 Hz. After treatment, the dielectric constant decreases gradually with increasing frequency, but the overall dielectric constant remains lower than before treatment. At 100 Hz, the dielectric constant is 3.05, while at 1,000,000 Hz, it is 2.69. The comparison shows that at low frequencies, the difference in dielectric constants before and after treatment is small, indicating that the material already has good electrical properties at low frequencies. At high frequencies, the dielectric constant after treatment is significantly lower than before treatment, indicating that electrothermal post-treatment significantly improves the material's insulation properties at high frequencies. This may be because the denser and more ordered cross-linked network after electrothermal post-treatment restricts dipole reorientation polarization, especially under high-frequency electric fields. Furthermore, the reduction in FVF and improved filler-matrix interface reduce the accumulation of interfacial space charge (interfacial polarization), which is a dominant polarization mechanism in composites at these frequencies. The results show that post-treatment systematically reduces the di-

electric constant across the entire test frequency range, with particularly significant improvements at high frequencies.

Table 3: Comparison of dielectric constants

Frequency/Hz	Dielectric constant before processing	Dielectric constant after processing
100	3.12	3.05
200	3.08	3.01
500	3.05	2.98
1000	3.02	2.95
2000	2.99	2.92
5000	2.96	2.89
10,000	2.93	2.86
50,000	2.89	2.82
100,000	2.85	2.78
200,000	2.82	2.75
500,000	2.79	2.72
1,000,000	2.76	2.69

A decrease in dielectric constant is typically accompanied by an improvement in bulk insulation performance. As shown in **Table 4** and **Figure 11**, both the insulation resistance and breakdown voltage of the material are significantly improved. The average insulation resistance before treatment is 250.6 ± 0.9 MΩ, indicating that the material itself has good insulation performance. The average insulation resistance after treatment is 310.7 ± 1.2 MΩ, which is significantly higher than the value before treatment. Meanwhile, the pre-treated material already has a high insulation resistance, indicating that it has good insulation performance in its untreated state. After treatment, the insulation resistance is significantly improved, indicating that electrothermal post-treatment further enhances the insulation performance of the material. A comparison of the pre- and post-treatment results shows that the insulation resistance of all the samples tested after treatment is higher than before treatment. The range of change is also relatively consistent, indicating that electrothermal post-treatment significantly and stably improves the material's insulation performance.

Table 4: Comparison of insulation resistance values before and after electrothermal post-treatment

Sample number	Insulation resistance before treatment (M)	Insulation resistance after treatment (M)
1	250.3	310.7
2	248.9	308.5
3	252.1	312.3
4	249.7	309.2
5	251.5	311
6	250.8	310.5
7	249.2	308.8
8	251.9	312.1
9	250.6	310.9
10	249.5	309.4
Average ± SD	250.6 ± 0.9	310.7 ± 1.2

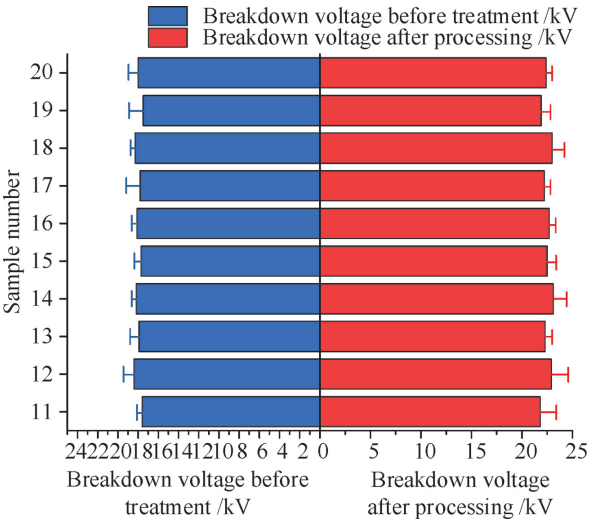

Figure 11: Comparison of breakdown voltage before and after treatment

To further evaluate its tolerance under strong electric fields, the study tests the breakdown voltage of the material (as shown in **Figure 11**). The average breakdown voltage before treatment is 18.0 ± 0.3 kV. After treatment, the average breakdown voltage significantly increases to 22.5 ± 0.4 kV, an increase of 25 %. This indicates that electrothermal post-treatment significantly enhances the dielectric strength of the material. Notably, despite the substantial increase in breakdown strength, the data scatter remains minimal. Statistical analysis indicates a high Weibull modulus ($\beta > 60$) for both pre- and post-treatment states. This confirms that the electrothermal post-treatment maintains the exceptional uniformity and reliability of the material network while elevating its insulation limit.

These systematic improvements in electrical properties ultimately trace back to the densification of the microstructure. As quantitatively revealed by the MD simulations in this study, higher crosslinking degrees lead to a significant reduction in the system's FVF, from 5.8 % to 4.1 %. At the microscopic level, this means that the migration pathways for potential charge carriers (such as impurity ions) are effectively compressed and blocked, resulting in an increase in the activation energy required for their transition. Macroscopically, this manifests as a decrease in electrical conductivity. However, insulation resistance and breakdown strength are significantly enhanced, providing a fundamental physical explanation for the enhanced electrical properties.

4 DISCUSSION AND INTERPRETATION

The results of this study clearly indicated that precisely controlled electrothermal post-treatment was not a traditional thermal-aging process, but rather an efficient structural annealing process. Its core mechanism used the precise transport of thermal energy to transition the metastable polymer network to a more stable, lower-en-

ergy state with a more orderly structure, thereby releasing the material's inherent performance potential.

The comparison of models with CD increased from 78 % to 92 % in MD simulation provided a direct microscopic explanation for the enhancement of macroscopic performance. A denser and more uniform crosslink network could more effectively disperse and transfer external stress, avoiding stress concentration at local defects, thereby delaying the initiation and propagation of microcracks. This was directly reflected in the significant increase in tensile strength (+44.7 %) and modulus. Similarly, the increase in Tg and improvement in thermal stability was a direct consequence of the restricted movement of molecular chains in a stronger binding network. This was consistent with the free volume theory of polymers. According to this theory, the increase in Tg was essentially a macroscopic manifestation of the need for molecular chain segments to overcome higher energy barriers in order to move in concert. Meanwhile, the decrease in FVF, as calculated by MD simulation, provided direct microscopic evidence of this phenomenon. The optimization of electrical properties also stemmed from this. Higher crosslink density reduced the mobility of polar groups, while the decrease in FVF directly hindered carrier migration, collectively leading to improved dielectric properties and insulation strength.

It is essential to situate these findings within the broader context of recent advancements in silicone rubber modification to highlight the distinct advantages of the proposed electrothermal post-treatment.

First, regarding the thermal mechanism: Our findings offer a crucial distinction from the thermal aging study by Su et al.[3] While they reported a significant degradation in tensile strength and elongation due to uncontrolled thermal stress (aging), our study demonstrates that a precisely controlled electrothermal treatment acts as a constructive structural žannealing' process. This process utilizes thermal energy within a controlled kinetic window to drive residual functional groups to complete reactions, thereby simultaneously enhancing stiffness and ductility rather than causing degradation.[3,16]

Second, regarding the complexity-performance trade-off: Current research primarily relies on formulation-centric approaches. For instance, the addition of bio-fillers like cuttlebone[4] or metallic oxides such as chromium oxide[6] can improve radiation shielding or thermal stability. However, as noted in the review by Leong et al.,[8] these exogenous additives often face challenges related to filler agglomeration and poor interfacial compatibility, which can compromise mechanical flexibility. Similarly, while Xie et al.[9] achieved high conductivity through magnetic field-induced graphene alignment, the process requires complex dynamic magnetic field equipment. In sharp contrast, our endogenous optimization strategy achieves remarkable increases, +44.7 % in tensile strength and +25 % in breakdown voltage, without introducing any new components or complex external fields, maintaining the material's purity and uniformity.[17]

Finally, in terms of industrial application: Unlike production process optimizations based on machine learning,[7] which primarily focus on manufacturing efficiency and yield rates, our method unlocks the intrinsic material potential post-molding. This suggests that electrothermal post-treatment offers a complementary yet distinct pathway, providing a more cost-effective and industrially scalable solution for manufacturing high-performance silicone rubber composites compared to complex additive manufacturing or extensive formulation redesigns.

Even though this study reaches some definitive conclusions, some topics still require more research. To allow for the specific tuning of material properties, future research should first thoroughly map the link between processing, structure, and property as a function of processing temperature, time, and cooling rate. Second, in the future, reaction force fields (such as ReaxFF) can be used to simulate the dynamic process of cross-linking reactions, providing deeper insights into the mechanism. Finally, to evaluate its long-term service performance and true reliability under extreme conditions, the material should be placed under composite aging conditions such as wet heat, high pressure, and multi-pulse electric fields.

5 CONCLUSION

This study conclusively demonstrates that electrothermal post-treatment is an efficient, simple physical strategy for optimizing the performance of composite insulating SR. This strategy combines MD simulation with systematic experiments. Research confirmed that post-processing optimized the microstructural network of the material, transforming it from a metastable state of insufficient cross-linking into a stable state of high cross-linking. This transformation was reflected in the model as an increase in crosslink density, from 78 % to 92 %. Post-processing also significantly reduced the FVF of the system, thereby improving its microstructural uniformity and density. This optimization of the microstructure directly leads to a comprehensive improvement in macro mechanical, thermal, and electrical properties. These findings provide profound microscopic insights into the thermal treatment modification mechanism of SR materials. More importantly, they demonstrate an endogenous optimization paradigm that transcends traditional additive formulation design. This approach precisely releases the intrinsic potential of materials through physical post-processing, offering new ideas and effective pathways for designing and manufacturing high-performance polymers.

6 REFERENCES

[1] Y. F. Gao, S. Li, S. J. He, X. W. Gu, Y. Q. Yue, Y. Chen, H. W. Zou, Z. B. Xing, Q. N. Liu, Molecular dynamics supported thermal-mois-

ture aging effects on properties of silicone rubber, Prog. Org. Coat., 192 (**2024**) 2, 108503–108518, doi:10.1016/j.porgcoat.2024.108503

[2] J. P. Liu, Y. W. Sun, J. S. Sun, K. H. Lv, N. Huang, Z. Xu, T. F. Zhang, Y. C. Li, G. S. Zhang, H. J. Yi, D. L. Hou, Research on Silicone Rubber Material as a Lost Circulation Material for Antarctic Drilling, SPE J., 30 (**2025**) 1, 144–151, doi:10.2118/223630-pa

[3] D. D. Su, Silicone rubber thermal aging performance for cables and accessories, J. Mater. Sci.-Mater. El., 35 (**2024**) 5, 328–339, doi:10.1007/s10854-024-12074-w

[4] G. Tochaikul, N. Tanadchangsaeng, A. Panaksri, N. Moonkum, Eco-friendly and low-dose radiation shielding material using natural waste cuttlebone and silicone rubber composite, Radiat. Phys. Chem., 231 (**2025**) 2, 112604–112618, doi:10.1016/j.radphyschem.2025.112604

[5] P. X. Yang, W. Yuan, H. W. Song, Effect of composite lattice on the high-temperature compressive behavior of silicone rubber based ablative materials, Compos. Struct., 344 (**2024**) 2, 118337–118348, doi:10.1016/j.compstruct.2024.118337

[6] H. M. Naguib, E. O. Taha, A. S. El-Deeb, M. M. A. Kader, M. A. Ahmed, Influence of chromium oxide nanoparticles and fiber fillers on silicone rubber nanocomposite, Polym. Bull., 81 (**2024**) 11, 9795–9812, doi:10.1007/s00289-024-05170-8

[7] Y. Yang, Optimization of Silicone Rubber Production Process Based on Machine Learning—A Case Study of Shenzhen Xiongyu Rubber Hardware Products Co., Ltd, Innov. Sci. Technol., 4 (**2025**) 4, 96–103, doi:10.63593/IST.2788-7030.2025.05.012

[8] Y. L. Leong, H. N. Lim, I. Ibrahim, Graphene in rubber formulations: a comprehensive review and performance optimization insights, Mol. Syst. Des. Eng., 8 (**2023**) 10, 1229–1251, doi:10.1039/d3me00082f

[9] J. K. Xie, Q. Zhou, J. X. Guo, H. Yin, Z. Hao, Z. Luo, Y. H. Xu, L. Yang, R. H. He, Preparation of Conductive Silicone-Rubber Composites by Dynamic Magnetic Field-Induced Orientation of Ferrosoferric Oxide-Loaded Reduced Graphene Oxide, ACS Appl. Polym. Mater., 6 (**2024**) 10, 5684–5695, doi:10.1021/acsapm.4c00314

[10] V. Kumar, M. N. Alam, S. S. Park, Review on functionalized CNTs reinforced silicone rubber composites for potential wearable applications, Polym. Compos., 45 (**2024**) 14, 12503–12529, doi:10.1002/pc.28664

[11] Z. Y. Xue, X. L. Geng, X. Li, Y. Q. Cao, J. L. Zhang, A. Aydeng, J. Liu, Compressive mechanical properties of lattice structures filled with silicone rubber, Mech. Adv. Mater. Struct., 31 (**2024**) 27, 9062–9072, doi:10.1080/15376494.2023.2265354

[12] L. Long, Y. B. Cai, X. F. Chi, Y. Chen, Z. G. Heng, H. W. Zou, L. W. Yan, M. Liang, A novel molecular structure design of liquid silicone rubber modified by ceramic precursors for high-performance flexible ablation, Polym. Degrad. Stabil., 225 (**2024**) 2, 110775–110789, doi:10.1016/j.polymdegradstab.2024.110775

[13] J. M. Dhivakar, S. Kornhuber, R. Sarathi, Enhanced Mechanical, Thermal, and Erosion Resistance Properties via the Synergetic Effect of n-ATH/LMGP Added Ceramifiable Silicone Rubber Composites for Electrical Insulation, Silicon, 16 (**2024**) 5, 1917–1928, doi:10.1007/s12633-023-02802-y

[14] A. Jurásková, S. M. Olsen, K. Dam-Johansen, M. A. Brook, A. L. Skov, Reliable Condensation Curing Silicone Elastomers with Tailorable Properties, Molecules, 26 (**2021**) 1, 82, doi:10.3390/molecules26010082

[15] T. Bardelli, C. Marano, F. Briatico-Vangosa, Influence of curing thermal history on cross-linking degree of a polydimethylsiloxane: Swelling and mechanical analyses, Express Polym. Lett., 16 (**2022**) 9, 924–932, doi:10.3144/expresspolymlett.2022.67

[16] B. X. Du, Y. P. Hou, X. X. Kong, Q. Fu, Dielectric, Mechanical, and Breakdown Properties of Liquid Silicone Rubber Under Different Thermal Aging Conditions, IEEE T. Dielect. El. In., 32 (**2025**) 1, 273–280, doi:10.1109/tdei.2025.3527431

[17] Y. L. Dong, X. Y. Yuan, High-efficiency electrothermal and electromagnetic interference shielding performance of expanded graphite/silicone film, Polym. Compos., 46 (**2025**) 1, 506–514, doi:10.1002/pc.29002